Amazon River plume influence on Western Tropical Atlantic dynamic variability

H. L. Varona, D. Veleda, M. Silva, M. Cintra, Moacyr Araujo

Amazon River plume influence on Western Tropical Atlantic dynamic variability

H.L. Varona[a,*], D. Veleda[a], M. Silva[a], M. Cintra[b], M. Araujo[a,c]

[a] Department of Oceanography, DOCEAN, Federal University of Pernambuco, Recife, PE, Brazil
[b] Federal University of Rio Grande do Norte, Natal, RN, Brazil
[c] Brazilian Research Network on Global Climate Change, Rede CLIMA, S. José dos Campos, SP, Brazil

Abstract:

This study focuses on analysing the potential impact of the Amazon and Pará Rivers on the salinity, temperature and hydrodynamics of the Western Tropical North Atlantic (WTNA) region between 60.5°–24 °W and 5 °S–16 °N.The Regional Ocean Model System (ROMS) was used to simulate ocean circulation with 0.25° horizontal resolution and 32 vertical levels. Two numerical experiments were performed considering river discharge and river input. Temperature and salinity distributions obtained numerically were compared with Simple Ocean Data Assimilation (SODA) and in situ observations from the Prediction Research Moored Array in the Tropical Atlantic (PIRATA) buoys located at 38 °W8 °N and 38 °W12 °N. Surface currents were compared with Surface Currents from Diagnostic model (SCUD). Once we verified that model results agreed with observations, scenarios with and without river discharges were compared. The difference between both simulations in the Sea Surface Temperature distribution was smaller than 2 °C, whereas the Sea Surface Salinity (SSS) changed by approximately 8 psu in the plume area close to the coast from August to December and reaching SSS differences of approximately 4 psu in the region of the North Equatorial Counter Current (NECC). The surface current velocities are stronger in the experiment with river discharge, mainly in the NECC area from September to December and close to the coast in June to August. The results show that river discharges also cause a phase shift in the zonal currents, anticipating the retroflection of the North Brazil Current by two months and enhancing eastward NECC transport, which is in agreement with observations. The Mixed Layer Depth and Isothermal Layer Depth in the presence of river discharge is 20–50 m shallower over the entire extension of the Amazon plume compared with the situation without continental inflows. As a consequence, stronger Barrier Layers develop in the river plumes, reducing the Oceanic Heat Content in the WTNA.

Keywords: ROMS Western Tropical North Atlantic Amazon River discharge Oceanic heat content Mixed layer Ocean circulation Barrier layer

1. Introduction

The circulation in the Western Tropical North Atlantic Ocean (WTNA) performs an important role in the interhemispheric transport of mass, heat, and salt and in the thermohaline overturning cell (Schmitz and McCartney, 1993; Bourlès et al., 1999a; Silva et al., 2009a; Veleda et al., 2012). Furthermore, a strong western boundary current, the North Brazil Current (NBC) is the main conduit for cross-equatorial transport of South Atlantic upper-ocean water as part of the Atlantic meridional overturning cell (Johns et al., 1998). This current flows north westward, intercepting the Amazon and Pará River freshwater discharges along the Brazilian

north coast.

The WTNA is a region with a complex system of zonal currents and counter-currents forced by subtropical gyres and the action of the trade winds in both hemispheres (Stramma et al., 2005). The NBC is considered a low latitude strong western-boundary current (Garzoli et al., 2004; Fratantoni and Richardson, 2006; Akuetevi and Wirth, 2015), and it is periodically retroflected near 6–8 °N and separated away from the boundary, turning anti-cyclonically for more than 90°, and forming anticyclonic eddies exceeding 450 km in overall diameter (Richardson et al., 1994; Garzoli et al., 2004; Fratantoni and Richardson, 2006). The NBC retroflection feeds the North Equatorial Counter Current (NECC), an eastward zonal current that contributes to the formation of the anticyclonic current rings (Castelão and Johns, 2011). The NBC rings are a significant contributor to transporting water across current gyres and between hemispheres in the tropical Atlantic (Bourlès et al., 1999a; Johns et al., 1998; Schott et al., 2003; Stramma et al., 2005).

The WTNA is also a region with intense land-ocean interaction, characterised by complex material transport, mixed layer depth changes (Grodsky et al., 2012; Coles et al., 2013) and high biogeochemical activity (Lefèvre et al., 2010; Ibánhez et al., 2017; Araujo et al., 2014, 2017), giving rise to alterations in local and remote oceanic processes. For example, river discharge use to be a small component of the open ocean salinity balance, but the magnitude of the Amazon freshwater source is so important that the discharged volume reaches two-fold the net evaporation minus precipitation budget over the north western tropical Atlantic (Ferry and Reverdin, 2004). Thus, in addition to the physical and weather/climate impacts, the Amazon and Pará Rivers also inject terrestrially derived sediments, nutrients, and coloured as well as transparent dissolved organic matter that can also be traced thousands of kilometres from the river mouth (Hu et al., 2004). The Biological community structure is strongly influenced by these terrigenous inputs of dissolved organic matter and nutrients, as well as by the induced changes in the stratification in the upper ocean (Stukel et al., 2014), leading to a globally significant uptake of atmospheric carbon dioxide in the river plume area (Cooley et al.2007; Ibánhez et al., 2015, 2016, Lefèvre et al., 2017).

The Amazon River plume flows into the WTNA near the equator and is carried north westward along the Brazilian shelf by the NBC (Müller-Krager et al., 1988; Salisbury et al., 2011). This is the main source of freshwater in the world, with an average discharge of approximately 222,800 m^3s^{-1} , it deposits almost 20% of the global river discharge onto the equatorial Atlantic Ocean continental shelf (Goulding et al., 2003; Barthem et al., 2004). The Amazon River plume extends thousands of kilometres over the North Atlantic Ocean arriving at the Caribbean Sea (Müller-Karger et al., 1989; Johns et al., 1990). Strong seasonal variations in this current system occur in response to trade wind variability and seasonal migration of the atmospheric Intertropical Convergence Zone (ITCZ) between its southern position in boreal winter, and its northern position in boreal summer (Xie and Carton, 2004). This leads to northward transport of Amazon waters in boreal winter, and eastward transport of Amazon water in the NECC in boreal spring through autumn (Müller-Krager et al., 1988; Lentz, 1995; Fratantoni and Glickson, 2002; Coles et al., 2013; Foltz et al., 2015). Thus, the influence of Amazon water is felt far from the river mouth through enhancement of surface stratification leading to the formation of barrier layers (Silva et al., 2005; Ffield, 2007; Coles et al., 2013; Grodsky et al., 2014). Thus, the Amazon River plume is thought to influence the surface ocean heat balance and its interaction with the atmosphere in the WTNA.

Several recent studies have used in situ observation data, satellite products, general circulation models (OGCMs) and regional models to explain the spatial and temporal variability of the Amazonian plume and its interaction with the NBC rings (Fratantoni and Glickson, 2002; Ffield, 2007; Korosov et al., 2015). For example, Schmidt et al. (2011) implemented an operational forecasting system, that use a high-resolution model to resolve the migration rate of the NBC rings, on a short time scale. Other recent work links the intensification of hurricanes to the spreading of Amazonian freshwater discharges due to the impact of haline stratification on reduction of the vertical heat flux (Balaguru et al., 2012; Grodsky et al., 2012; Newinger and Toumi, 2015) and the periodic movement of the NBC rings (Ffield, 2007).

In this work, we used a climatological modelling approach to investigate the role of the Amazon and Pará River plumes on the circulation and thermohaline variability in the Amazon River-Ocean continuum (Araujo et al., 2017). Two numerical experiments were conducted, contrasting the scenarios with and without the contribution of continental freshwater to the tropical Atlantic. We focused here on the impact of river inflows on the circulation (NBC-NECC system) and temperature/salinity distribution,which induce important changes in isothermal/mixed/barrier layer formation and oceanic heat content in the Western TropicalNorth Atlantic Ocean. The model configuration, simulation scenarios, observational dataset and analysis procedures are described in Section 2. In addition to simulation considering the discharges of the Amazon and Pará Rivers in the presence of islands (Scenario RRF), an idealised configuration without continental contributions was also simulated (Scenario NRF). The results from scenario RRF are compared with the available observational datasets in order to validate the simulation. Then, differences between two scenarios are examined. Simulation results, including model validation, are presented and discussed in Section3. The last section provides the conclusions and outcome perspectives of this work.

2. Data and methodology

2.1. Numerical modelling experiments

In this work, we use the Regional Ocean Modeling System (ROMS), an open source software, which has been continuously developed by a large community of scientists, with more than 400,000 lines of FORTRAN code. ROMS integrates the primitive Reynolds equations in a rotational free-surface system using the Boussinesq approximation, the hydrostatic approximation and the balance of vertical momentum (Shchepetkin and McWilliams, 2005; Song and Haidvogel, 1994; Panzer et al., 2013). This was adapted to different geographic regions of the world where good results were obtained (Haidvogel et al., 2000; Penven et al., 2000; Silva et al., 2009a; Tchamabi et al., 2017).

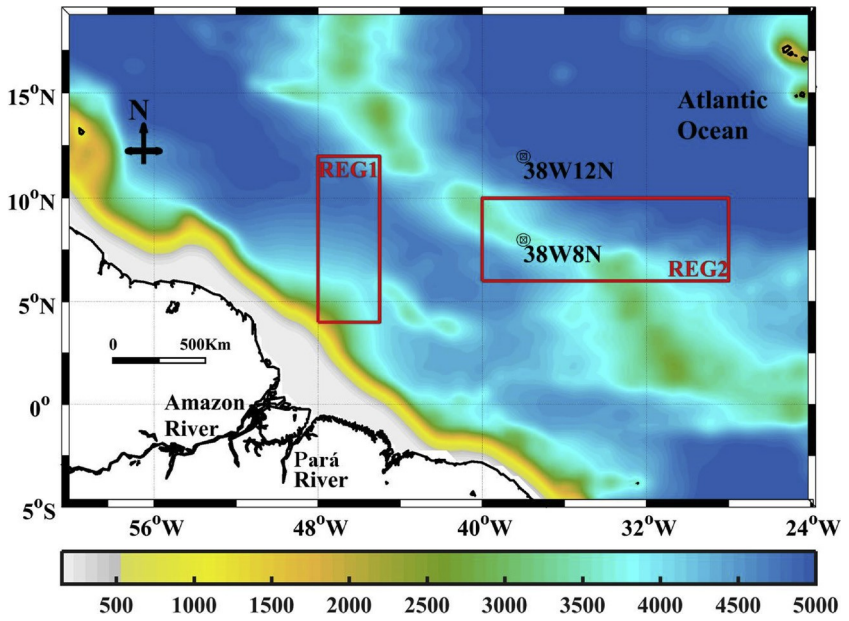

Fig. 1. The model domain framed in 60.5°-24 °W/5 °S-16 °N. The colour bar represents ocean bathymetry and the red rectangles correspond to two regions used for model validation: REG1 (48-45 °W/4–12 °N) and REG2 (40-28 °W/6–10 °N). PIRATA buoys at 38 °W8 °N and 38 °W12 °N are also indicated in the figure.

The region of study is framed in 60.5°-24 °W and 5 °S-16 °N (Fig. 1) with 0.25° of resolution (approximately 27.8 km), covering an area of $4916 \cdot 10^3 km^2$ corresponding to a 183 × 159 node grid with 32 levels in the vertical, 12 of which are in the upper 100 m and 20 in the 500 m. The ETOPO2 (Smith and Sandwell, 1997) topography database was used in the vertical discretisation with 2min of resolution. The red rectangles in Fig. 1 indicate the regions used to evaluate model performance where strong seasonal changes in ocean circulation and thermohaline structure are observed; REG1 corresponds to the NBC retroflection region, and REG2 represents the NECC area. The locations of PIRATA buoys are also plotted in the figure.

Four lateral boundaries are considered open in simulations. In the lateral boundary and initial conditions all variables were constrained by the monthly mean of the 2009 World Ocean Atlas, WOA2009 (Locarnini et al., 2010; Antonov et al., 2010) with a resolution of 1°. The surface forcings were obtained from the monthly mean climatology of the Comprehensive Ocean-Atmosphere Data Set (COADS05) (Da Silva et al., 1994) with 0.5° of resolution. Tides are an important process in mixing the river freshwater plumes with the open ocean and are obtained from the TPXO7 (Egbert et al., 1994; Egbert and Erofeeva, 2002), which has altimetry data from several satellites to improve the accuracy of the results obtained through the hydrodynamic model (Wang, 2004; D'Onofrio et al., 2012). The monthly mean river discharge was obtained from the Obidos and Tucurui gauge stations (Dai and Trenberth, 2002), and the monthly climatology of Sea Surface Temperature (SST) in the river discharge points was also obtained from WOA2009.

We performed two numerical experiments to estimate the potential impact of the Amazon and Pará Rivers on the salinity, temperature and surface currents of the WTNA. In the first experiment, hereafter referred to as River Runoff (RRF), the Amazon and Pará Rivers release freshwater into the WTNA. Given the geographical configuration of the Amazon River Delta, there are four inputs from the river to the WTNA (Fig. 2(a)): Canal do Norte, Baia de Santa Rosa, Canal Perigoso and Canal do Jurupari. The inputs are

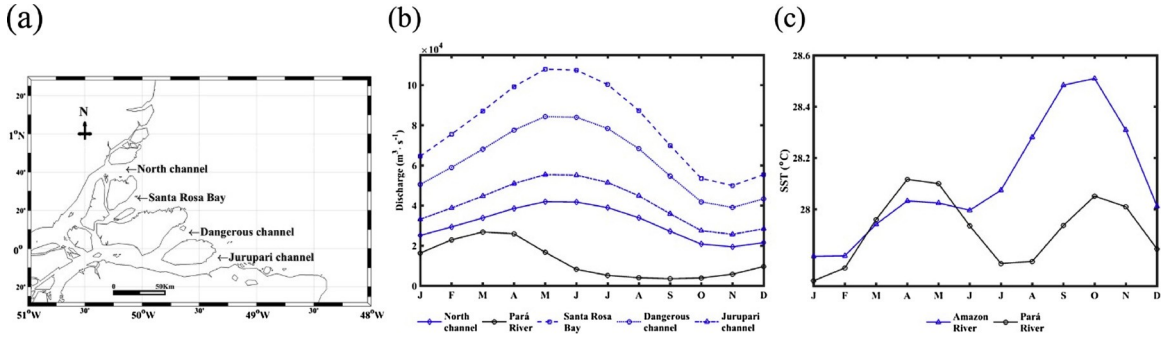

Fig. 2. (a) Location map of the Amazon River delta and its four inputs (North channel, Santa Rosa Bay, Dangerous channel and Jurupari channel) from the river to WTNA. (b) Monthly distribution of discharge ($m^3 s^{-1}$) of the Amazon River (blue lines) and Pará River (black line), from the Obidos and Tucuruí gauge stations. (c) Monthly distribution of temperature (ºC) of the Amazon River (blue line) and Pará River (black line).

placed in four cells of the grid. Considering the channel width, the contribution was calculated for each one, distributed as 14.47%, 37.27%, 29.13% and 19.13%, respectively (Fig. 2(b)), with the same monthly temperature distribution for the four input nodes in the Amazon River Delta and different in the input node of the Pará River (Fig. 2(c)). In the second experiment, the No-River Runoff (NRF), the Amazon and Pará Rivers do not release freshwater into the WTNA, keeping the same model parametrisation and initial and boundary conditions. We ran each experiment for 11 years (spin-up), but our analyses are focused on the last simulation year.

2.2. Mixed layer depth (MLD), isothermal layer depth (ILD), barrier layer thickness (BLT) and oceanic heat content (OHC) criteria

The MLD was defined as the depth where the density increases from the surface value due to a prescribed temperature decrease of 0.2 °C ($\Delta T = -0.2°C$) while maintaining constant surface salinity. The MLD was mathematically defined by Sprintall and Tomczak (1992) and de Boyer Montégut et al. (2007) as

$$\Delta\sigma = \sigma(T + \Delta T, S, P_0) - \sigma(T, S, P_0)$$

where Δσ is the density difference for the same change in temperature ΔT at constant salinity (Δσ = 0.125 kg m-3 (Monterey and Levitus, 1997)), T and S are the values of temperature and salinity at the reference depth (Z_{REF}) and P_0 is the pressure at the ocean surface. The ILD is the depth at which the temperature is equal to $T + \Delta T$. In this study, we consider Z_{REF}= 0, corresponding to the SST obtained in simulations.

The Barrier Layer (BL) may prevent heat exchange between the oceanic mixed layer (MLD) and deeper water, influencing the SST and ensuring greater isolation along the Mixed Layer Depth (MLD). The thicker the BL is, the less heat exchange exists between deep cold water and the oceanic mixed layer. The BLT is calculated as

$$BLT = ILD\text{-}MLD$$

The transfer of mass, momentum and energy through the mixing layer is an important feature influencing oceanic circulation and changes with the atmosphere. The ILD determines the heat content and the mechanical inertia of the layer that interacts directly with the atmosphere (de Boyer Montégut et al., 2004). Changes in oceanic heat content play an important role in sea level rise due to thermal expansion. The quantity of energy stored per unit area in the ocean (OHC) between levels Z_{REF} and h is defined according to Jayne et al. (2003) as

$$OHC = \rho_0 C_p \int_{Z_{REF}}^{h} T(z)dz$$

where OHC is Oceanic Heat Content in Jm^{-2}, ρ_0= 1025 kg m^{-3} is the representative density of seawater at the sea surface, $C_p = 4 \cdot 10^3 J(kg - °C)^{-1}$ is the specific heat of seawater at constant pressure at the sea surface (Levitus et al., 2005), $T(z)$ is a vertical temperature, Z is Depth (m), Z_{REF}= 0 and h is the maximum depth to calculate the OHC.

As the depth increases, the temperature oscillation decreases and below the active ocean layer, there are practically no annual variations in temperature. The OHC is more related to the thickness of the isothermal layer than to the temperature directly; thus, we plan to study only the quantity of heat in the active layer of the ocean, numerically integrating the temperature in each vertical profile in the grids of the RRF and NRF experiments, from surface to $h = ILD$.

2.3. Model validation: comparison with observations

For model validation, we compare numerical SST and Sea Surface Salinity (SSS) variability with the Simple Ocean Data Assimilation (SODA) version 2.2.4 (Carton et al., 2000a, 2000b; Carton and Giese, 2008), which has a spatial resolution of 0.5° and integration period of 20 years (1991–2010).

Surface currents are compared with the Surface Current form Diagnostic model (SCUD) (Maximenko and Hafner, 2010), with spatial resolution of 0.5° and period of 2000-2008. To compare numerical results to previous findings reported by Richardson and Reverdin (1987), the average values of the zonal component of surface velocity were also calculated for two different regions of the NECC: the Western NECC (WNECC - 50-40 °W/5–8 °N), and the Eastern NECC (ENECC - 30-25 °W/5–8 °N).

Other than considering the overall differences between the RRF and NRF scenarios at the whole integration domain, the river induced circulation and thermohaline changes were examined at two highly dynamic areas of the WTNA (red rectangles in Fig. 1): (i) the REG1 region (48-45 °N/4–12 °N) corresponding to an NBC retroflection area; and (ii) the REG2 region (40-28 °W/6–10 °N), representing the zonal band NECC pathway.

Subsurface temperature and salinity distributions and variability obtained from the RRF scenario were compared to the observed climatology of the PIRATA buoys located at 38 °W8 °N and 38 °W12 °N (Servain et al., 1998; Bourlès et al., 2008), constructed during 2000-2015. The PIRATA mooring design allows high frequency measurements of ocean temperature at 11 levels (i.e., 1, 20, 40, 60, 80, 100, 120, 140, 180, 300, 500 m), salinity at 4 levels (1, 20, 40, 120 m), and meteorological variables at the sea surface, that are transmitted and kept immediately available on the Web after their validation (https://www.pmel.noaa.gov/gtmba/).

Except the previously mentioned comparison of the zonal component of current velocity, the results presented and discussed in the next section focus on the differences between the RRF and NRF experiments during: boreal winter (DJF: December, January, February); boreal spring (MAM: March, April, May), boreal summer (JJA: June, July, August) and boreal autumn (SON: September, October, November).

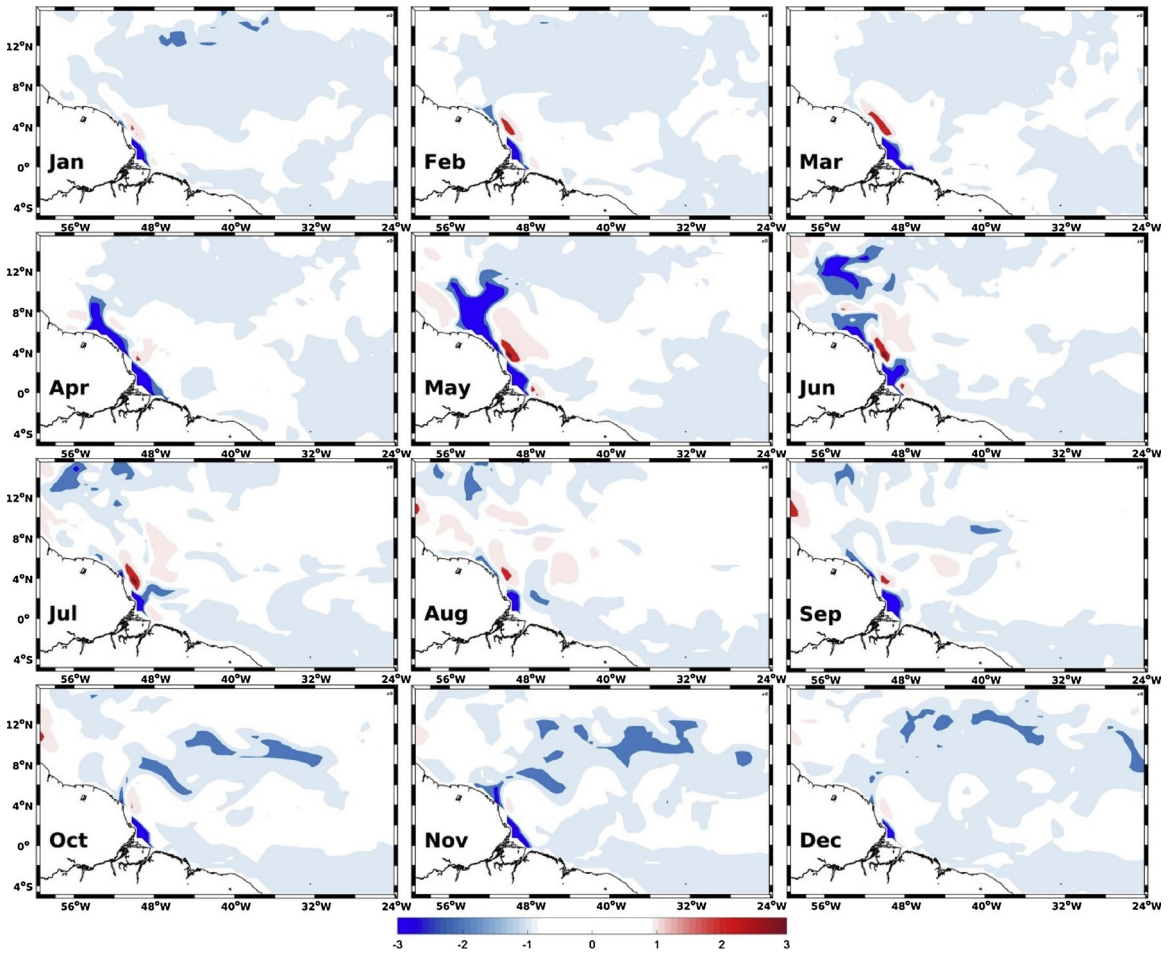

Fig. 3. Seasonal variability of the differences in SSS distributions (psu) between the RRF experiment and SODA climatology in the WTNA.

3. Results and discussion

3.1. Model evaluation: validation of the RRF experiment

The ROMS monthly climatology output is compared with the SODA dataset to evaluate modelresults and validate the RRF experiment. The differences in SSS between the model simulation and SODA climatology (RRF-SODA) are shown in Fig. 3. The results indicate that lower SSS values were obtained from ROMS simulations than from SODA in the area of the NBC retroflection (during April to June - boreal spring) and in some meanders of the NECC zonal corridor (during October to December - boreal autumn).

The differences between the SST climatology obtained from simulation and from SODA are shown in Fig. 4. The modelled mean SSTs present in general higher monthly averaged temperatures than SODA in the area of the NBC retroflection and the NECC, mainly during boreal autumn and early/mid-winter.

A comparison between seasonal averaged SSS (columns 1 and 2) and SST (columns 3 and 4) values obtained from simulations (RRF) and from SODA in REG2 area (NECC region, Fig. 1) is shown in Table 1. The mean value ± standard deviation is indicated in the first set of rows, and the range (minimum–maximum) in the second set for each season. The results indicate overall good agreement between SST and SSS generated by the RRF scenario and SODA. The maximum SSS difference in area REG2 (0.27 psu) is verified during boreal summer (June to August) and a minimum SSS difference (0.06 psu) during boreal spring (March to May). For SST, columns 3 and 4 in Table 1 show greater differences between RRF simulation and SODA in the REG2 area during boreal winter (December to February) (1.27 °C), when we still have the Amazon river plume feeding the NECC. The RRF simulation is better adjusted during boreal summer (June to August).

Fig. 5 shows the comparison between near surface (0–120 m depth for salinity and 0–500 m depth for temperature) seasonal variation of the vertical distributions of temperature and salinity obtained from the RFF scenario and from PIRATA observations at 38 °W8 °N and 38 °W12 °N. This figure indicates generally good agreement between model results and in situ measurements, but in order to have a statistical confirmation of model capacity to reproduce observations, we performed two-sample t-test. Prior to performing t-test, in situ and numerical profiles were normalised since the initial dataset showed non-normal distributions as verified

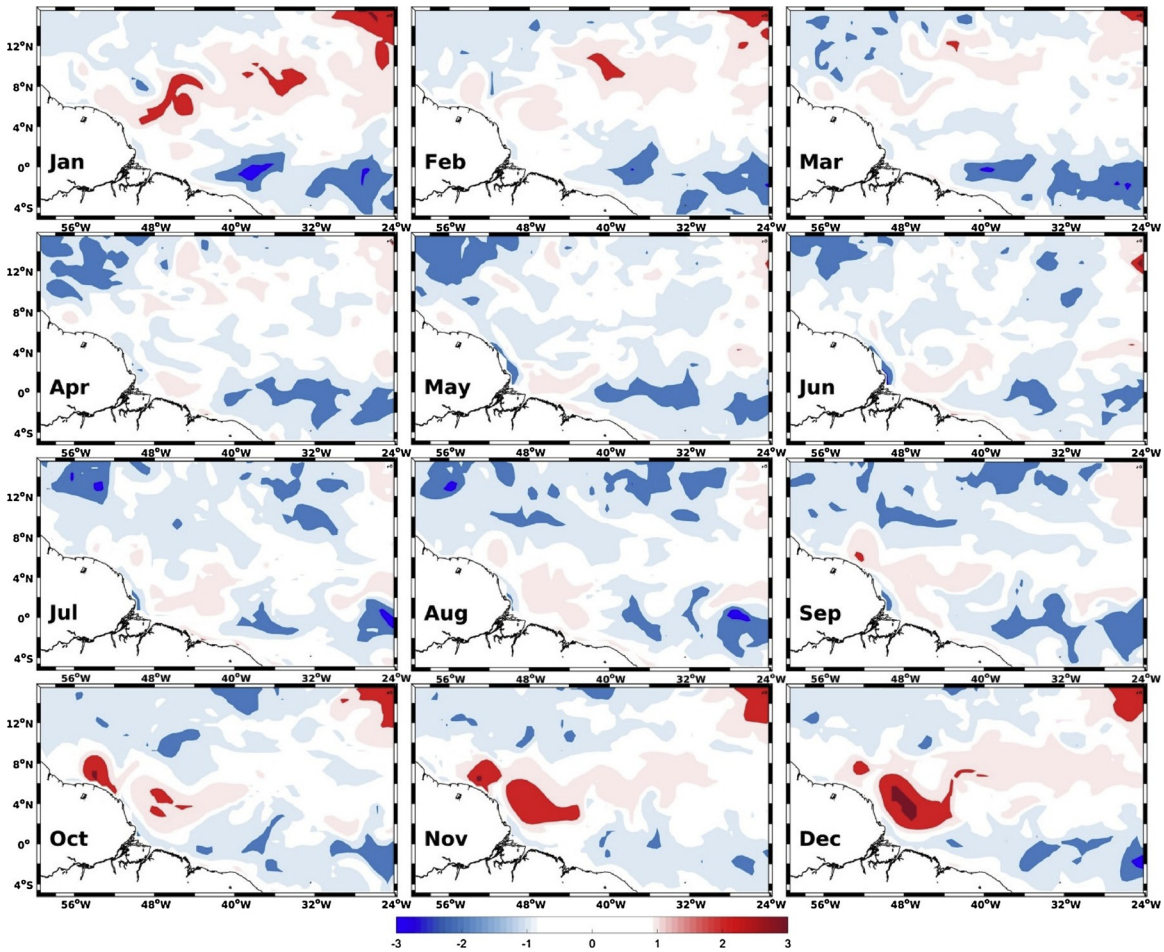

Fig. 4. Seasonal variability of the differences in SST distributions (°C) between the RRF experiment and SODA climatology in the WTNA.

Table 1
Comparison between seasonal SSS (columns 1 and 2) and SST (columns 3 and 4) values obtained from simulations (RRF scenario) and from SODA in the REG2 area (NECC region, Fig. 1). The mean value ± standard deviation is indicated in the first rows, and value ranges (minimum–maximum) in the second rows.

Period	SSS		SST	
	SODA (psu)	RRF (psu)	SODA (◦C)	RRF (◦C)
DJF	35.86 ± 0.02	35.63 ± 0.07	26.90 ± 0.04	28.17 ± 0.14
	(35.56–36.10)	(34.94–36.19)	(26.02–27.48)	(26.47–29.12)
MAM	36.09 ± 0.02	36.15 ± 0.01	26.74 ± 0.10	27.05 ± 0.27
	(35.87–36.32)	(35.81–36.47)	(25.60–27.61)	(25.73–28.31)
JJA	35.82 ± 0.03	36.09 ± 0.05	27.77 ± 0.07	27.77 ± 0.23
	(35.43–36.15)	(35.46–36.51)	(27.15–28.30)	(26.27–28.84)
SON	35.41 ± 0.07	35.23 ± 0.13	28.26 ± 0.04	28.63 ± 0.13
	(34.89–35.87)	(34.19–36.26)	(27.84–28.74)	(27.63–29.69)
Annual	35.79 ± 0.03	35.78 ± 0.08	27.42 ± 0.07	27.91 ± 0.19
	(35.44–36.11)	(35.10–36.36)	(26.65–28.03)	(26.53–28.99)

by the one-sample Kolmogorov-Smirnov test.

The simulated salinity at the position 38 °W8 °N (Fig.5(a)) shows a seasonal evolution of vertical structure similar to that observed from PIRATA data, in particular during boreal spring (August to December), when lower salinity Amazonian waters are transported eastward by the NECC. The main differences are verified from June to October, in the first 40 m, just after the beginning of NBC retroflection, when the freshwater river plume starts to feed the NECC (Coles et al.,2013; Grodsky et al., 2014). t-test indicated no statistically significant differences between vertical distributions of salinity issued from the RRF experiment and PIRATA

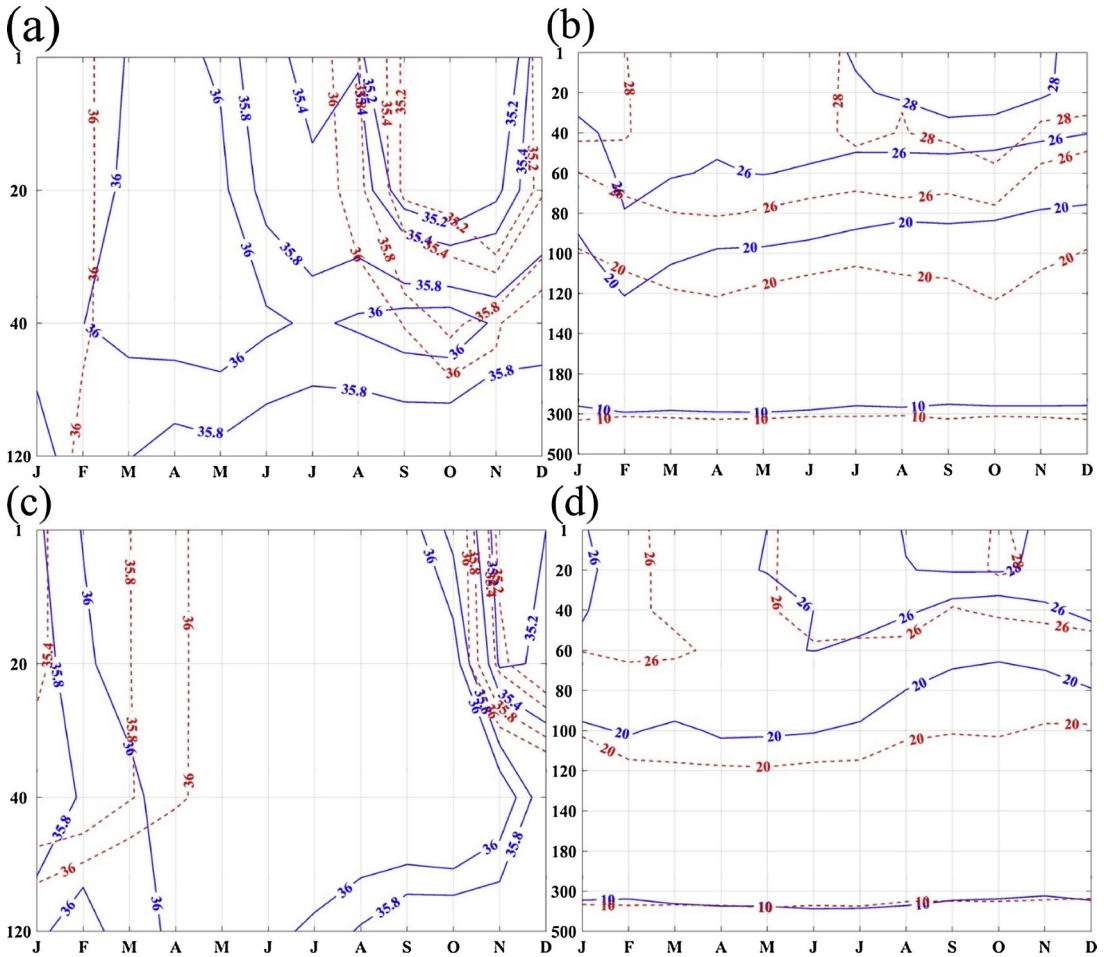

Fig. 5. Hovmöller diagrams of temperature and salinity obtained from model simulation (red dashed lines) and PIRATA observations (blue solid lines) at: 38 °W8 °N (a) salinity (psu) and (b) temperature (°C); and 38°W12°N (c) salinity (psu) and (d) temperature (°C).

data ($p = 0.9966$, $\alpha = 0.05$). The temperature evolution obtained numerically is also well adjusted to measurements (Fig. 5(b)), with no significant differences between the potential model and PIRATA data ($p = 0.8287$, $\alpha = 0.05$).

The vertical profiles of modelled salinity are in general agreement with in situ measurements at the position of the PIRATA buoy 38 °W12 °N (Fig. 5(c)). A mean difference of 0.4 psu is seen and no significant differences were found between model outputs and observations ($p = 0.9857$, $\alpha = 0.05$). The evolution of near surface vertical temperature structure is also similar to the measurement along the year (Fig. 5(d)), with some discrepancies between 100–120 m depth, just below the thermocline depth. Again, t-test indicated no significant differences between the model and measurements ($p = 0.8137$) for a significance level of 0.05.

The NECC is the main current transporting the Amazon River plume eastward (Grodsky et al., 2014). We now compare the seasonal evolution of the zonal components of surface velocity longitudinally averaged in the REG2 limits (40-28 °W) obtained numerically (RRF scenario) (Fig. 6(a)) to that issued from the SCUD dataset (Fig. 6(b)). Both cases show a gradual increase of the zonal component from July to October, between 4.0 and 10 °N, and decreasing during boreal autumn (September to November). The maximum difference between the model and SCUD was found between 5.5 and 6.5 °N in July and between 4 and 5 °N in October, with an averaged difference of 0.1 ms^{-1}. These results reveal that the model simulation represents the dynamics of the NECC variability in the WTNA quite well.

Finally, to compare model results to previous in situ observations, we calculated the averaged zonal component of surface velocity obtained numerically during boreal autumn at the WNECC and ENECC regions as 0.384 ms^{-1} and 0.226 ms^{-1}, respectively. These values are very close to those reported by Richardson and Reverdin (1987) for the same period and regions (0.410 ms^{-1} and 0.215 ms^{-1}, respectively).

3.2. Impact of river plumes: Comparison between the RRF and NRF experiments

In this section, we compare the seasonal evolution of the differences between the RRF and NRF scenarios (RRF-NRF). It aims to investigate the influence of river discharges on the surface ocean circulation and thermohaline structure in the WTNA.

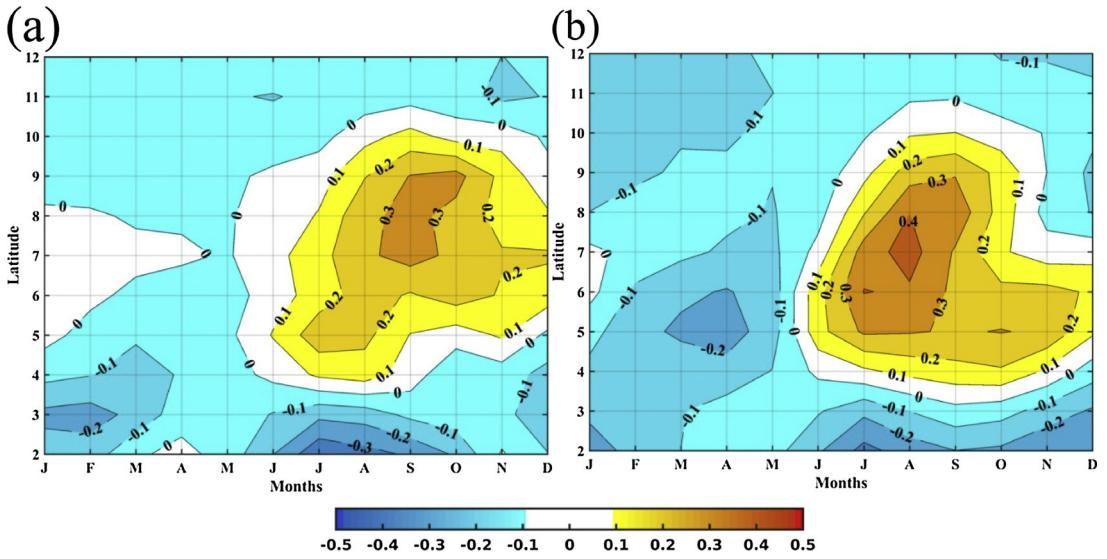

Fig. 6. Hovmöller diagrams of the zonal component of surface velocity longitudinally averaged in the REG2 limits (40-28 °W): (a) Model (RRF) simulation; (b) SCUD dataset.

3.2.1. Impacts of thermohaline structure and changes on ILD, MLD, BLT and OHC

Fig. 7(a) shows the seasonal variation of the difference of SSS distributions in the WTNA obtained from model results with (RRF) and without (NRF) the Amazon and Pará River discharges. The RRF experiment shows lower salinity confined to the coast from December to February. From March to May, the RRF scenario shows evidence of lower salinity at the NBC retroflection area. From June to August, the plume spreads northward, and from September to November, the plume is transported eastward by the NECC. The river scenario shows 10–12 psu lower salinity values along the coast than does the NRF case, which represents the seasonal cycle of the Amazon plume well. In the NECC area, the continental inflows generate lower SSS values of 4 psu. These results are in agreement with previous observations and modelling efforts (Silva et al., 2009b, 2010; Coles et al., 2013; Korosov et al., 2015; Newinger and Toumi, 2015; Araujo et al., 2017). These authors shows exist seasonal change in SSS influenced by river plume (Silva et al., 2009a,b, Silva et al., 2010; Araujo et al., 2017), and that subsurface temperature is influenced by river freshwater due the formation of BLT (Newinger and Toumi, 2015).

Fig. 7(b) shows the differences in seasonal SST distributions for both situations (RRF-NRF). Although not significant, the results indicate that river discharges induce a warming near the Amazon River mouth, in particular during boreal spring/summer and at the NBC retroflection area in boreal autumn. A small cooling is also verified very close to the coastline at the left side of the river mouth. In the open ocean SST changes are not very sensitive to the river inputs. These results are in agreement with previous observations (Silva et al., 2010; Newinger and Toumi, 2015; Araujo et al., 2017). These authors shows no exist significant changes in SST influenced by river plume, except near Amazon mouth controlled by freshwater temperature (Newinger and Toumi, 2015). Changes in temperature and salinity distributions due to the inflow of Amazon and Pará River freshwater modify the thickness and evolution of the Isothermal (ILD), Mixed (MLD) and Barrier layers (BLT) in the WTNA. Fig. 8(a) indicates that oceanic mixed layers are shallower in the RRF experiment than in the situation simulated with no-river input. These changes are located in the regions (and periods) where (when) river plumes spread into the WTNA. Indeed, the low-density layer formed by the freshwater river discharge induces MLD 20 m–50 m shallower over the entire extension of the plume. The MLD minimum for the RRF experiment is 6 m throughout the year and the maximum fluctuates between 88 m and 100 m, being deeper in the SON period. In contrast, whereas minimum MLD values are approximately 6 m, the maximum mixed layer depth oscillates between 100 m and 120 m in the absence of river plumes (NRF experiment).

Fig. 8(b) shows the spatial distribution of the differences in the seasonally averaged distributions of ILD between the RRF and NRF experiments. Although less intense than MLD, we also find shallower ILDs in the presence of river discharges than in the simulations without continental contribution (NRF), in particular during boreal summer (JJA) and autumn (SON). As expected, there is a clear influence of SST changes over the ILD, being up to 1 °C higher in the plume area for the RRF scenario than for the No-rivers simulation (Fig. 7(b)).

As presented for MLD and ILD, Fig. 8(c) shows the spatial distribution of the seasonally averaged differences of BLT distributions between the RRF and NRF experiments. The discharge of freshwater from the rivers plays a fundamental role in the formation of barrier layers along the extensions of the river plume spreading into the WTNA. The maximum difference in BLT is verified at the Amazon mouth extending north westward when the river plume is transported towards the Caribbean Sea. During boreal autumn (SON) the differences in BLT extend to the east following plume transport by the NECC. In the absence of rivers, the BL is almost non-existent in the plume area, and we find 100% of the BLT in the range of 1–35 m. In the RRF experiment the BLT reaches 82–94 m in the DFJ, MAM and JJA periods and up to 110 m in boreal autumn (SON). Similar magnitudes and BLT distributions were reported by

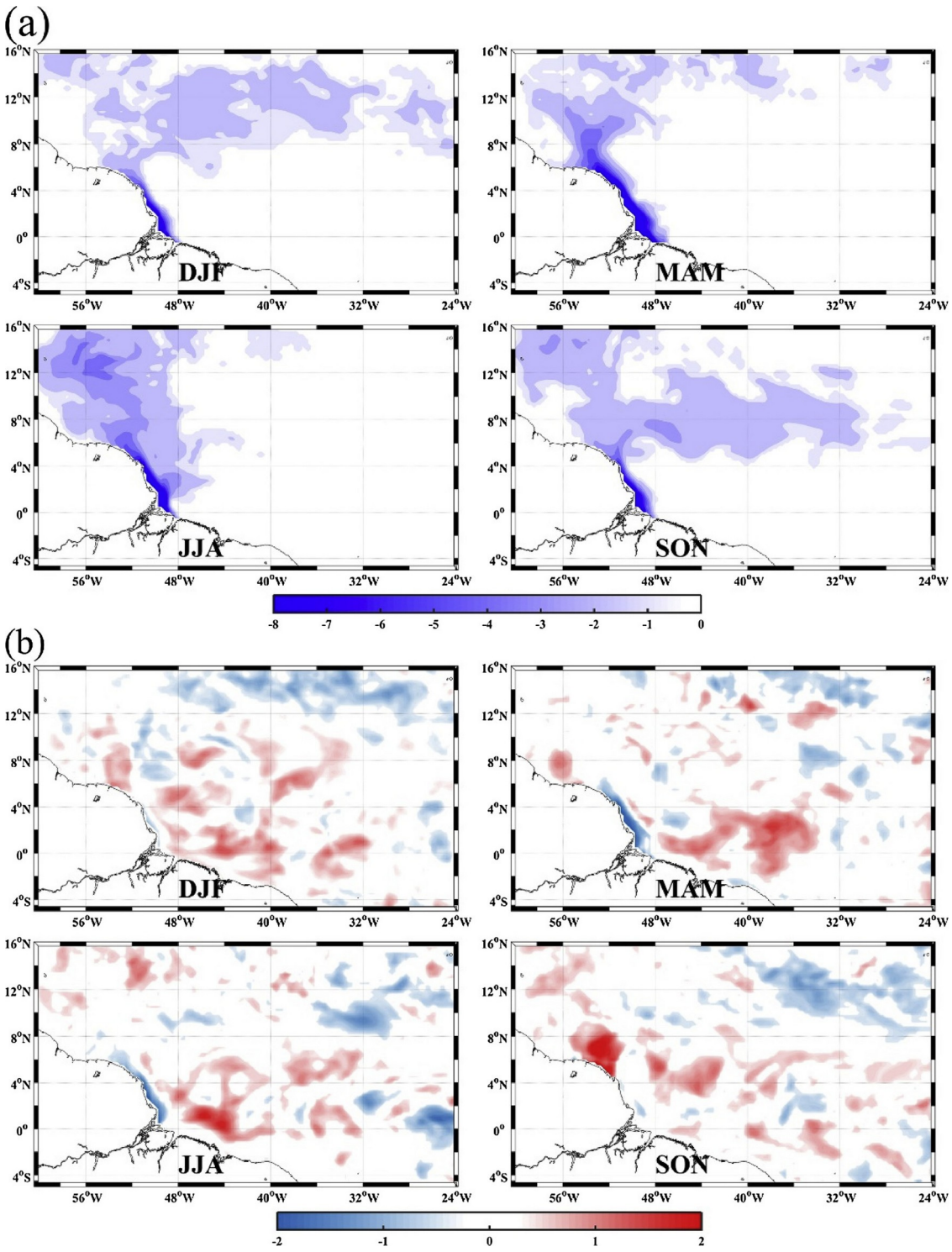

Fig. 7. Seasonal evolution of the difference of: (a) SSS (psu); and (b) SST (^{o}C) between the RRF (River discharges) and NRF (No-river discharges) simulations during boreal winter (DJF: December, January, February), boreal spring (MAM: March, April, May), boreal summer (JJA: June, July, August), and boreal autumn (SON: September, October, November).

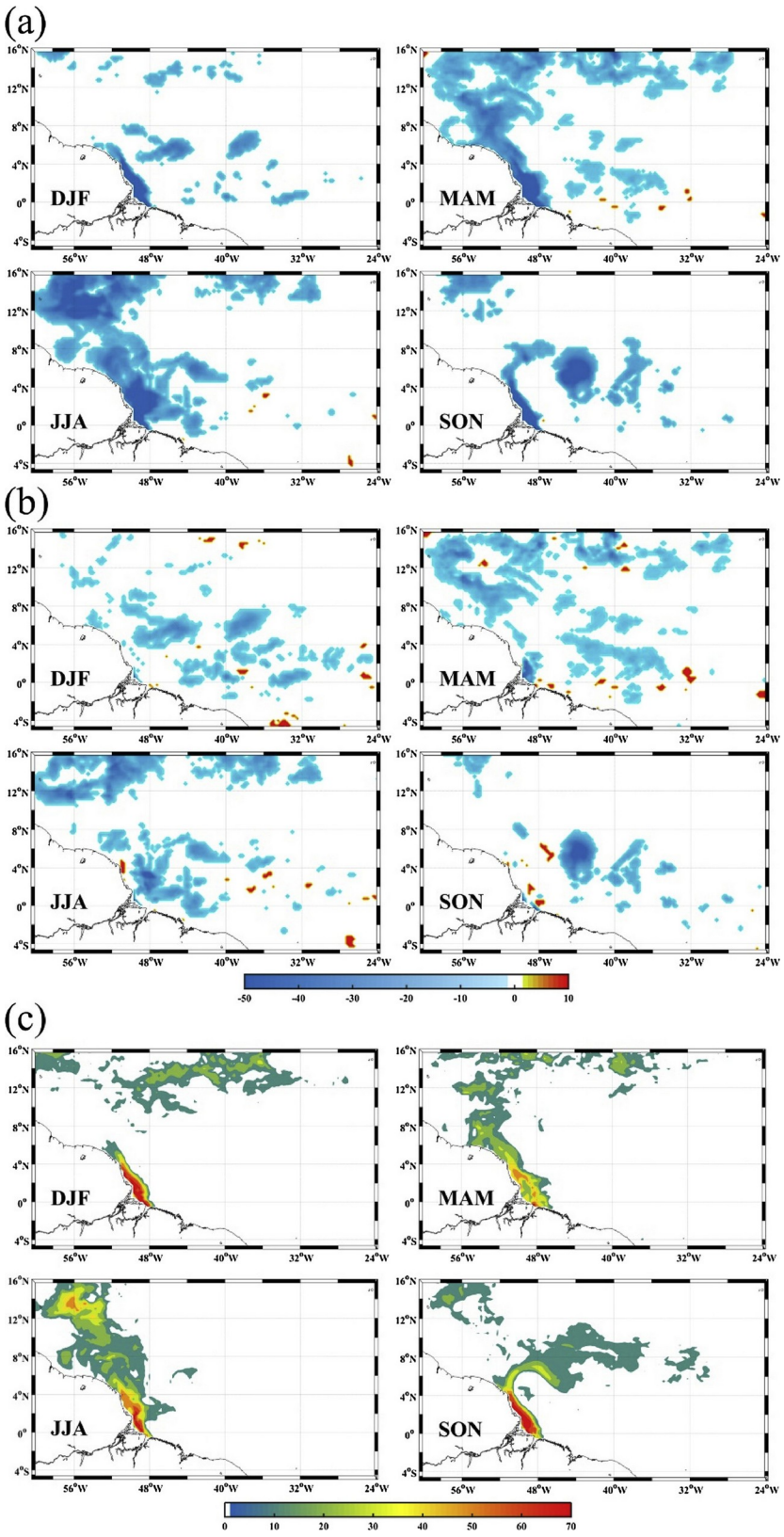

Fig. 8. Seasonal evolution of the difference of: (a) MLD (m), (b) ILD (m), and (c) BLT (m) between the RRF (River discharges) and NRF (No-river discharges) simulations during boreal winter (DJF: December, January, February), boreal spring (MAM: March, April, May), boreal summer (JJA: June, July, August), and boreal autumn (SON: September, October, November).

the in situ observations of Pailler et al. (1999) and Silva et al. (2005, 2009b and 2010).

It is expected that space and time modifications to temperature distribution due to river inflows should also induce changes in oceanic heat content (OHC) in the WTNA. Simulation results indicate that higher accumulations of heat in the ILD without rivers varied from 1.1 to $1.3 \cdot 10^{0} J m^{-2}$, whereas the maximum values of OHC in the RRF experiment ranged from 1.0 to $1.2 \cdot 10^{0} J m^{-2}$. Fig. 9 presents the seasonally averaged differences in OHC between the simulations with and without rivers (RRF-NRF) indicating that rivers reduce oceanic heat storage, in particular along the plume spreading areas. The largest differences ranged between −0.7 and $-0.3 \cdot 10^{0} J m^{-2}$, during the periods of MAM, JJA and SON, confirming that variation in ILD is the main factor influencing the OHC difference between the RRF and NRF experiments.

3.2.2. Impact on ocean circulation and changes to NBC and NECC

Fig. 10 shows the differences in ocean surface circulation between numerical results obtained from the RRF and NRF scenarios. The seasonal cycle provides evidence of the rivers' impact on the WTNA regions under the influence of freshwater plumes (NBC retroflection and NECC areas). The differences showed in Fig. 10 evidence the action of freshwater input increasing the pressure gradient near Amazon/Pará mouths. Horizontal density and Sea Surface Height gradients (not shown here) increase the geostrophic transport of NBC component, north of Amazon mouth and also increase the intensity of the anticyclonic ring along the year. Even when the Amazon inflow is weak (Fig. 10, period DJF), pressure differences caused by input river freshwater induce zonal transport along 4 °N to compensate the increase of NBC transport near coast.

Stronger surface velocities are present from June to November and a well-defined meandering/ring. The structure is highlighted from September to November. These differences (reaching 1 $m s^{-1}$) emphasize the role of the Amazon river plume in the dynamics of the NBC-NECC system, including NBC retroflection, formation of NBC rings and eastward NECC meandering/transport.

To evaluate the influence of Amazon inflow on the dynamics of the NBC retroflection we compare the evolution of the longitudinally averaged (REG1 limits 48-45 °W) zonal component of the surface currents obtained from the RRF and NRF experiments (Fig. 11(a) RRF and (b) NRF). The results show overall similar patterns in both simulations with the zonal current intensity reaching a maximum of 0.5 ms^{-1}. In both cases, stronger zonal velocity appears in January-February (between 7° and 8 °N), with a core of less intense but still significant eastward transport centred at 9 °N in March-April. However, during the second half of the year, when river discharges are stronger (Goulding et al., 2003; Barthem et al., 2004; Araujo et al., 2014), there is evidence for differences in the space and time evolution of zonal currents between the RRF and NRF scenarios. Although eastward currents start to occur in the middle of August in both scenarios, stronger and broader eastward transport is verified when the Amazon and Pará Rivers are considered. The

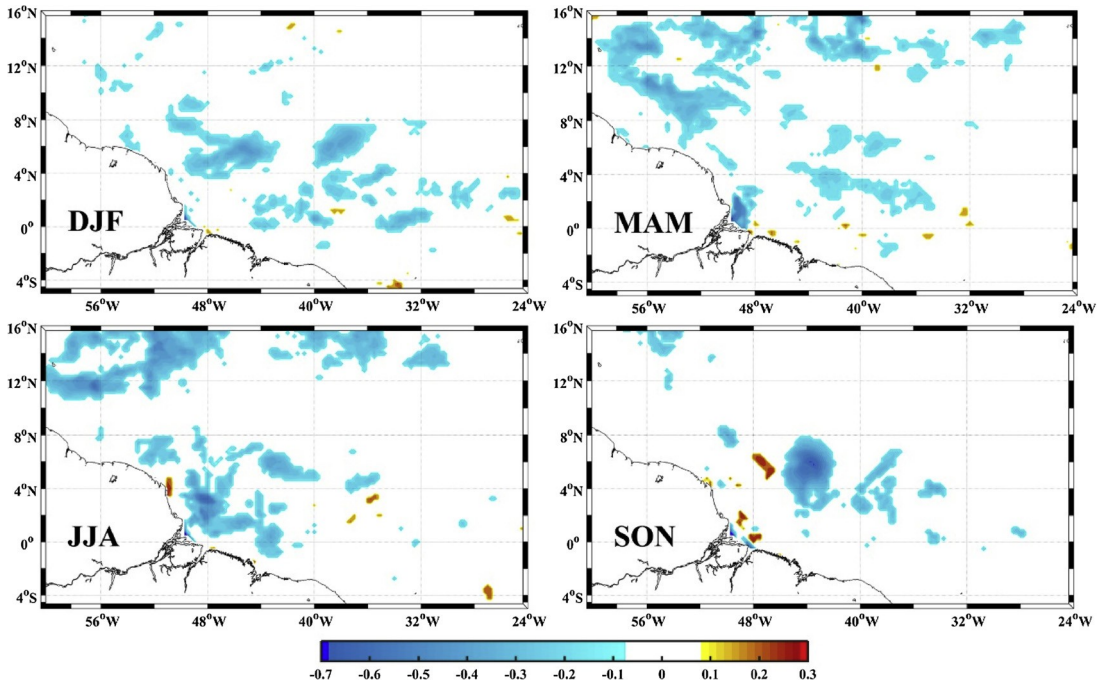

Fig. 9. Mean seasonal cycle of difference in OHC (J m^{-2}) integrated from Z_{REF} to ILD. Boreal winter (DJF: December, January, February), boreal spring (MAM: March, April, May), boreal summer (JJA: June, July, August), and boreal autumn (SON: September, October, November).

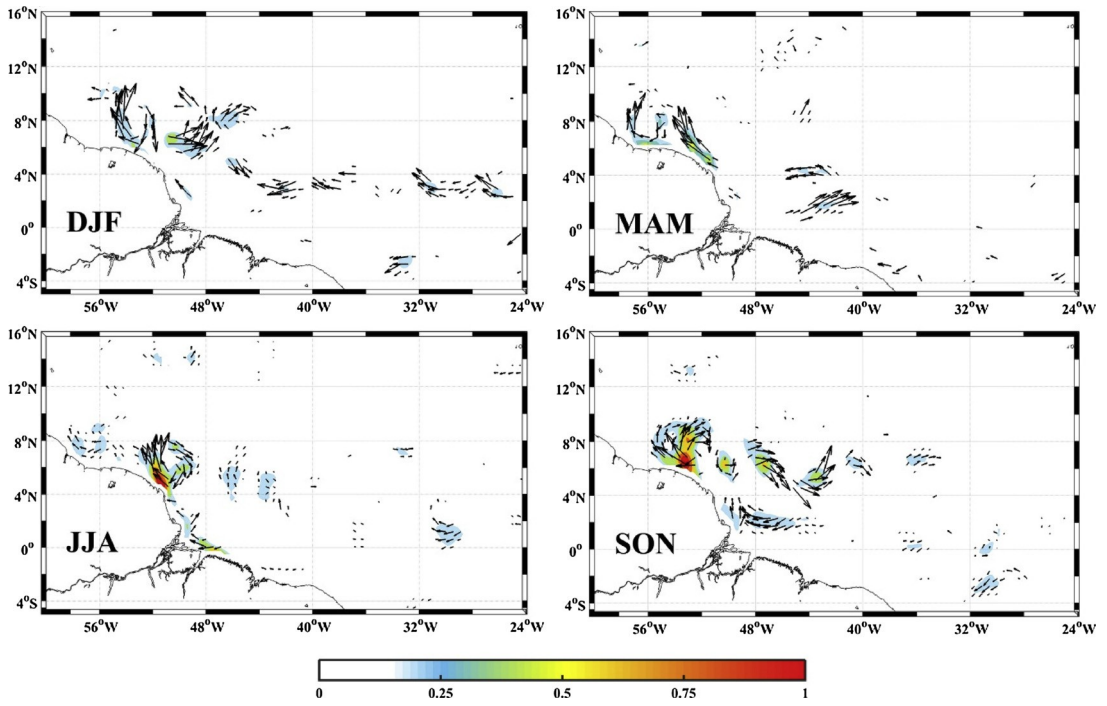

Fig. 10. Seasonal evolution of the difference in surface currents (ms $^{-1}$) between the RRF (River discharges) and NRF (No-river discharges) simulations during boreal winter (DJF: December, January, February), boreal spring (MAM: March, April, May), boreal summer (JJA: June, July, August), and boreal autumn (SON: September, October, November).

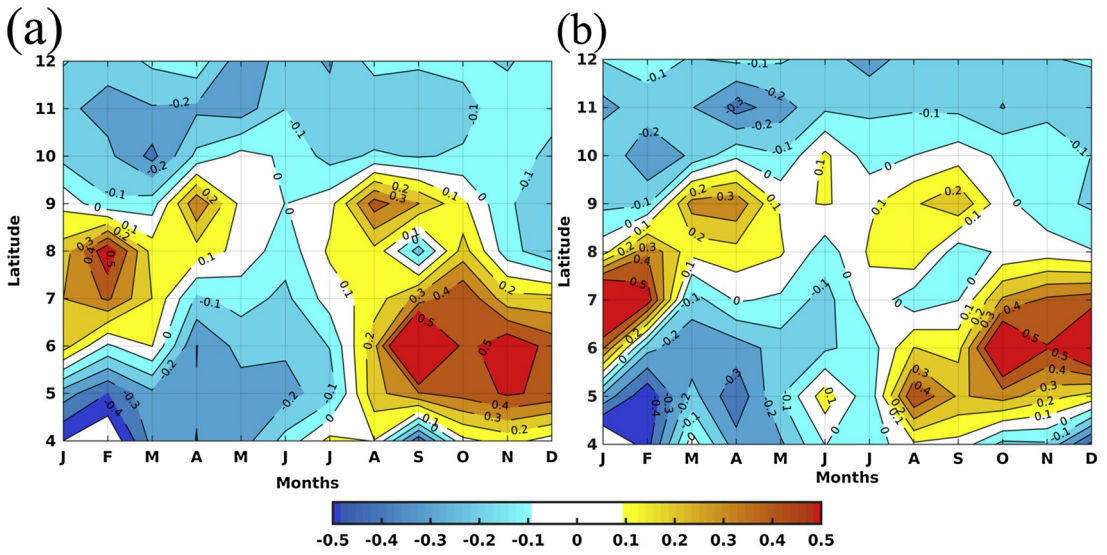

Fig. 11. Hovmöller diagrams of the zonal component of surface velocity longitudinally averaged in the REG1 limits (48-45 °W): (a) RRF scenario (River discharges); (b) NRF scenario (No-river discharges).

period of maximum zonal current values is also different for both situations, whereas the cores of high eastward velocity are verified since the beginning of August in the RRF simulation; those maximum values are shifted to mid-September in the NRF case. The differences in intensity and space-time evolution of the zonal surface currents in the second part of the year reveals how river plumes change ocean circulation in the WTNA, in particular over the NBC retroflection area and the NECC pathway (see also Fig. 10).

4. Conclusions

This study uses observations and numerical modelling to investigate the influence of the Amazon and Pará Rivers discharge on

the surface ocean circulation and thermohaline variability in the Western Tropical North Atlantic Ocean (WTNA). Regional climatological modelling is used to conduct two numerical experiments with (RRF) and without (NRF) continental freshwater inflow. Our analyses focused on the impact of rivers on the circulation (NBC-NECC system) and temperature/salinity distribution that induce changes in the isothermal/mixed/barrier layer formation and oceanic heat content.

The model results considering real situations (with rivers) are in good agreement with previous observations and reanalysis efforts, showing similar patterns of thermohaline distribution and ocean surface circulation in the WTNA. The rivers' impact on SSS variability is evident. The space and time variability of SSS in the area of the NBC retroflection and NECC is clearly identified, showing a confinement of the lower salinity waters near the coast from December to February and spreading eastward along the NECC pathway from September to November. The SSS fields change near the Amazon River mouths, reducing the salinity by approximately 8 psu.

A warm core of SST is concentrated at the left side of the Amazon mouth from September to November, following the NBC retroflection area, due to the influence of warmer river temperature. However, in the open ocean, SST changes are not significantly sensitive to river discharges.

The computed differences between the RRF (Rivers discharges) and NRF (No-rivers discharges) scenarios indicate a strong impact of river plumes on ocean circulation in the WTNA. Compared to the NRF experiment, the RRF experiment increases the surface current up to 1 ms^{-1} . Stronger velocity occurs from June to November and well-defined meandering/ring generation structures are highlighted from September to November. Pressure terms, associated with horizontal density gradients, seems to be reinforced in RRF (River discharges) scenarios near coast, increasing intensity of the NBC - NECC system. The results also emphasize the role of the Amazon plume in the dynamics of the NBC retroflection, as well as in the eastward NECC transport. The comparisons of longitudinally averaged zonal components of surface currents in the NBC retroflection area for the RRF and NRF experiments show overall similar patterns during the first half of the year, when river discharges are lower. However, during the second semester, the beginning of maximum eastward transport (zonal currents reaching 0.5 ms^{-1}) is two months delayed in the absence of continental inflows, and is also weaker and limited to a narrower latitude band compared to the observed RRF scenario.

The Amazon and Pará Rivers also impact the isothermal/mixed/barrier layer dynamics in the WTNA. Induced MLD and ILD are 20–50 m shallower over the entire extension of the river plumes when river discharges are considered, resulting in the maximum BLT at the river mouths, extending north westward as the plume is transported towards the Caribbean during boreal spring and summer. Higher values of BLT are observed along the zonal NECC pathway during boreal autumn, after eastward NBC retroflection.

Changes in near surface thermohaline structure drive oceanic heat content. The results indicate that modifications in isothermal/mixed/barrier layers due to river input result in less oceanic heat storage in the WTNA. Differences up to $0.1 \cdot 10^{0} Jm^{-2}$ are verified in the large portion of the Western Tropical North Atlantic occupied by less salty plume waters.

In summary, the results indicate the Amazon and Pará Rivers' discharges impact the thermohaline structure in the WTNA as follows: (i) modifying seasonal salt distribution variability in the river plume area, (ii) inducing shallower Mixed and Isothermal layers as a response to salinity changes, (iii) enhancing Barrier Layer formation and increasing its depth, and (iv) reducing Ocean Heat storage capacity. Furthermore, ocean surface circulation is modified by the following factors: (v) anticipating the NBC retroflection (by about two months), and (vi) enhancing the eastward NECC transport/spreading of low salinity water into the central tropical Atlantic.

Considering all the evidence for the influence of the Amazon and Pará Rivers on the dynamics of the WTNA Ocean, it seems interesting as a next step to investigate the effects of these physical alterations and of the riverine nutrient and organic material contributions on the biogeochemical cycles of the Western Tropical North Atlantic region. In this case, in addition to the analyses of observations and in situ measurements, the use of coupled physical-biogeochemical modelling appears to be an exciting research method to be explored.

Acknowledgements

The first author thanks to Human Resources Program (PRH-47) of the Agência Nacional do Petróleo (ANP) for the concession of PhD scholarships. This paper is a contribution of the Brazilian Research Network on Global Climate Change, FINEP/ Rede CLIMA Grant Number 01.13.0353-00. The authors thank to the Brazilian National Institute of Science and Technology for Tropical Marine Environments–INCT AmbTropic (CNPq/FAPESB grants 565054/2010-4 and 8936/2011), Brazilian Research Network on Global Climate Change – Rede CLIMA (FINEP grants 01.13.0353-00), the Project Simulating the Amazon River Plume and its Impact using Climate Models, Grant CAPES-TAMU 003440/2015-00, the Project Modeling the light field in the waters of Equatorial Atlantic under the effects of the Amazon River discharge: implication to biogeochemical processes and primary production, MEC/MCTI/CAPES/CNPq/FAPs Grant: 401326/2012-8; D. V. thanks to Project ProdPluma – Modelo Regional de Produtividade PrimÃária da Pluma do Amazonas (CNPq grant 460687/2014-0).

References

Akuetevi, C.Q.C., Wirth, A., 2015. Dynamics of turbulent western-boundary currents at low latitude in a shallow-water model. Ocean. Sci. 11, 471–481. https://doi.org/10.5194/os-11-471-2015.

Antonov, J., Seidov, D., Boyer, T., Locarnini, R., Mishonov, A., Garcia, H., Baranova, O., Zweng, M., Johnson, D., 2010. World Ocean Atlas 2009. In: In: Levitus, S. (Ed.), Salinity, vol. 2. NOAA Atlas NESDIS 69, pp. 184.

Araujo, M., Noriega, C.E.D., Lefèvre, N., 2014. Nutrients and carbon fluxes in the estuaries of major rivers flowing into the tropical Atlantic. Front. Mar. Sci. 1, 10. https://doi.org/10.3389/fmars.2014.00010.

Araujo, M., Noriega, C., Hounsou-Gbo, G.A., Veleda, D., Araujo, J., Bruto, L., Feitosa, F., Flores-Montes, M., Lefèvre, N., Melo, P., Otsuka, A., Travassos, K., Schwamborn, R., Neumann-Leitão, S., 2017. A synoptic assessment of the amazon river-ocean continuum during boreal autumn: from physics to plankton communities and carbon flux. Front. Microbiol. https://doi.org/10.3389/fmicb.2017.01358.
Balaguru, K., Chang, P., Saravanan, R., Leung, L.R., Xu, Z., Li, M., Hsieh, J.S., 2012. Ocean barrier layers' effect on tropical cyclone intensification. Proc. Natl. Acad. Sci. 109, 14343–14347.
Barthem, R.B., Charvet-Almeida, P., Montag, L.F.A., Lanna, E., 2004. Amazon Basin, GIWA Regional Assessment 40b. UNEP.
Bourlès, B., Molinari, R.L., Johns, E., Wilson, W.D., Leaman, K.D., 1999a. Upper layer currents in the western tropical North Atlantic (1989-1991). J. Geophys. Res. 104, 1361–1375.
Bourlès, B., Lumpkin, R., McPhaden, M.J., Hernandez, F., Nobre, P., Campos, E., Yu, L., Planton, S., Busalacchi, A.J., Moura, A.D., Servain, J., Trotte, J., 2008. The PIRATA program: history, accomplishments, and future directions. Bull. Am. Meteorol. Soc. https://doi.org/10.1175/2008BAMS2462.1.
Carton, J.A., Giese, B.S., 2008. A reanalysis of ocean climate using Simple Ocean Data Assimilation (SODA). Mon. Weather. Rev. 136, 2999–3017. https://doi.org/10.1175/2007MWR1978.1.
Carton, J.A., Chepurin, G., Cao, X., 2000a. A Simple Ocean Data Assimilation Analysis of the Global Upper Ocean 1950–95. Part I: Methodology. J. Phys. Oceanogr. 30, 294–309. https://doi.org/10.1175/1520-0485.
Carton, J.A., Chepurin, G., Cao, X., 2000b. A Simple Ocean Data Assimilation Analysis of the Global Upper Ocean 1950–95. Part II: Results. J. Phys. Oceanogr. 30, 311–326. https://doi.org/10.1175/1520-0485.
Castelão, G.P., Johns, W.E., 2011. The sea-surface structure of North Brazil Current Rings derived from shipboard and moored acoustic Doppler current profiler observations. J. Geophys. Res. 116.
Coles, V.J., Brooks, M.T., Hopkins, J., Stukel, M.R., Yager, P.L., Hood, R.R., 2013. The pathways and properties of the Amazon river plume in the tropical North Atlantic Ocean. Journal of Geophysical Research C: Oceans 118, 6894–6913.
Cooley, S.R., Coles, V.J., Subramaniam, A., Yager, P.L., 2007. Seasonal variations in the Amazon plume-related atmospheric carbon sink. Global Biogeochem. Cycles 21, 1–15.
D'Onofrio, E., Oreiro, F., Fiore, M., 2012. Simplified empirical astronomical tide model—an application for the Río de la Plata estuary. Comput. Geosci. 44, 196–202.
Da Silva, A., Young, A.C., Levitus, S., 1994. Atlas of sur face marine data 1994. Algorithms and Procedures. Technical Report 6, vol. 1 NOAA, NESDIS.
Dai, A., Trenberth, K.E., 2002. Estimates of freshwater discharge from continents: latitudinal and seasonal variations. J. Hydrometeorol. 3, 660–687. https://doi.org/10.1175/1525-7541.
de Boyer Montégut, C., Madec, G., Fischer, A.S., Lazar, A., Iudicone, D., 2004. Mixed layer depth over the global ocean: an examination of profile data and a profile-based climatology. J. Geophys. Res. 109, C12003.
de Boyer Montégut, C., Mignot, J., Lazar, A., Cravatte, S., 2007. Control of salinity on the mixed layer depth in the world ocean: 1. General description. J. Geophys. Res. Oceans 112.
Egbert, G.D., Erofeeva, S.Y., 2002. Efficient inverse modeling of barotropic ocean tides. J. Oceanic Atmos. Technol. 19, 183–204.
Egbert, G.D., Bennett, A.F., Foreman, M.G.G., 1994. TOPEX/POSEIDON tides estimated using a global inverse model. J. Geophys. Res. Oceans 99, 24821–24852.
Ferry, N., Reverdin, G., 2004. Sea surface salinity interannual variability in the western tropical Atlantic: An ocean general circulation model study. J. Geophys. Res. Oceans 109, 1–11. https://doi.org/10.1029/2003JC002122.
Ffield, A., 2007. Amazon and Orinoco River Plumes and NBC Rings: Bystanders or Participants in Hurricane Events? J. Clim. 20, 316–333.
Foltz, G.R., Schmid, C., Lumpkin, R., 2015. Transport of surface freshwater from the equatorial to the subtropical north Atlantic Ocean. J. Phys. Oceanogr. 45, 1086–1102.
Fratantoni, D.M., Glickson, Da., 2002. North Brazil Current Ring Generation and Evolution Observed with SeaWiFS*. J. Phys. Oceanogr. 32, 1058–1074.
Fratantoni, D.M., Richardson, P.L., 2006. The evolution and demise of North Brazil Current rings. J. Phys. Oceanogr. 36, 1241–1264.
Garzoli, S.L., Ffield, A., Johns, W.E., Yao, Q., 2004. North brazil current retroflection and transports. J. Geophys. Res. 109, 1–14.
Goulding, M., Barthem, R., Ferreira, E., 2003. Smithsonian Atlas of the Amazon, 1 edition. Smithsonian Institution Press.
Grodsky, S.A., Reul, N., Lagerloef, G., Reverdin, G., Carton, J.A., Chapron, B., Quilfen, Y., Kudryavtsev, V.N., Kao, H.Y., 2012. Haline hurricane wake in the Amazon/Orinoco plume: AQUARIUS/SACD and SMOS observations. Geophys. Res. Lett. 39, 4–11.
Grodsky, S.A., Reverdin, G., Carton, J.A., Coles, V.J., 2014. Year-to-year salinity changes in the Amazon plume: contrasting 2011 and 2012 Aquarius/SACD and SMOS satellite data. Remote Sens. Environ. 140, 14–22.
Haidvogel, D., Arango, H., Hedstrom, K., Beckmann, A., Malanotte-Rizzoli, P., Shchepetkin, A., 2000. Model evaluation experiments in the North Atlantic basin: simulations in nonlinear terrain-following coordinates. Dyn. Atmos. Ocean. 32, 239–282.
Hu, C., Montgomery, E.T., Schmitt, R.W., Muller-Karger, F.E., 2004. The dispersal of the Amazon and Orinoco River water in the tropical Atlantic and Caribbean Sea: observation from space and S-PALACE floats. Deep. Sea Res. Part Ii Top. Stud. Oceanogr. 51, 1151–1171.
Ibánhez, J.S.P., Diverrès, D., Araujo, M., Lefèvre, N., 2015. Seasonal and interannual variability of sea-air CO 2 fluxes in the tropical Atlantic affected by the Amazon River plume. Global Biogeochem. Cycles 28 (9), 1–16. https://doi.org/10.1002/2015GB005110.
Ibánhez, J.S.P., Araujo, M., Lefèvre, N., 2016. The overlooked tropical oceanic CO 2 sink. Geophys. Res. Lett. 43 (8), 3804–3812. https://doi.org/10.1002/2016GL068020.
Ibánhez, J.S.P., Flores, M., Lefèvre, N., 2017. Collapse of the tropical and subtropical North Atlantic sink in boreal spring of 2010. Sci. Rep. 7, 41694. https://doi.org/10.1038/srep41694.
Jayne, S.R., Wahr, J.M., Bryan, F.O., 2003. Observing ocean heat content using satellite gravity and altimetry. J. Geophys. Res. Oceans 108. https://doi.org/10.1029/2002JC001619.
Johns, W., Lee, T., Schott, F., Zantopp, R., Evans, R., 1990. The North Brazil current retroflection: seasonal structure and eddy variability. J. Geophys. Res. 95, 22103–22120.
Johns, W.E., Lee, T.N., Beardsley, R.C., Candela, J., Limeburner, R., Castro, B., 1998. Annual cycle and variability of the North Brazil current. J. Phys. Oceanogr. 28, 103–128.
Korosov, A., Counillon, F., Johannessen, J.A., 2015. Monitoring the spreading of the Amazon freshwater plume by MODIS, SMOS, Aquarius, and TOPAZ. Journal of Geophysical Research C: Oceans 120, 268–283.
Lefèvre, N., Diverrès, D., Gallois, F., 2010. Origin of undersaturation in the western tropical Atlantic. Tellus B 62, 595–607.
Lefèvre, N., Montes, M.F., Gaspar, F.L., Rocha, C., Jiang, S., De Araújo, M.C., Ibánhez, J.S.P., 2017. Net heterotrophy in the Amazon continental shelf changes rapidly to a sink of CO2 in the outer Amazon plume. Front. Mar. Sci. 4, 278. https://doi.org/10.3389/fmars.2017.00278.
Lentz, S.J., 1995. The Amazon River Plume during AMASSEDS: subtidal current variability and the importance of wind forcing. J. Geophys. Res. C: Oceans 100, 2377–2390.
Levitus, S., Antonov, J., Boyer, T., 2005. Warming of the world ocean, 1955–2003. Geophys. Res. Lett. 32.
Locarnini, R., Mishonov, A., Antonov, J., Boyer, T., Garcia, H., Baranova, O., Zweng, M., Johnson, D., 2010. World Ocean Atlas 2009. In: In: Levitus, S. (Ed.), Temperature, vol. 1 US Gov. Print. Off., Washington, DC 184 pp.
Maximenko, N., Hafner, J., 2010. . SCUD: Surface CUrrents Form Diagnostic Model. IPRC Technical Note No. 5. International Pacific Research Center - School of Ocean and Earth Science and Technology - University of Hawaii. http://iprc.soest.hawaii.edu/users/hafner/NIKOLAI/SCUD/BAK/SCUD_manual_02_16.pdf.
Monterey, G., Levitus, S., 1997. Seasonal Variability of Mixed Layer Depth for the World Ocean, NOAA Atlas NESDIS 14. 100 pp.. NOAA, Silver Spring, Md.
Müller-Karger, F.E., McClain, C.R., Fisher, T.R., Esaias, W.E., Varela, R., 1989. Pigment distribution in the Caribbean Sea Observations from space. Prog. Oceanogr. 23, 23–64.
Müller-Krager, F.E., McClain, C.R., Richardson, P.L., 1988. The dispersal of the Amazons water. Nature 333, 56–59.
Newinger, C., Toumi, R., 2015. Potential impact of the colored Amazon and Orinoco plume on tropical cyclone intensity. J. Geophys. Res. Oceans 120, 1296–1317.
Pailler, K., Bourlès, B., Gouriou, Y., 1999. The barrier layer in the western tropical Atlantic Ocean. Geophys. Res. Lett. 26, 2069–2072.

Panzer, I., Lines, S., Mak, J., Choboter, P., Lupo, C., 2013. High Performance Regional Ocean Modeling With GPU Acceleration. IEEE/MTS OCEANS.
Penven, P., Roy, C., Colin de Verrdière, A., Largier, J., 2000. Simulation of a coastal jet retention process using a barotropic model. Oceanol. Acta 23, 615–634.
Richardson, P.L., Reverdin, G., 1987. Seasonal cycle of velocity in the Atlantic North Equatorial Countercurrent as measured by surface drifters, current meters, and ship drifts. J. Geophys. Res. Oceans 92, 3691–3708.
Richardson, P.L., Hufford, G.E., Limeburner, R., Brown, W.S., 1994. North brazil current retroflection eddies. J. Geophys. Res. 99, 5081–5093.
Salisbury, J., Vandemark, D., Campbell, J., Hunt, C., Wisser, D., Reul, N., Chapron, B., 2011. Spatial and temporal coherence between Amazon River discharge, salinity, and light absorption by colored organic carbon in western tropical Atlantic surface waters. J. Geophys. Res. 116, C00H02.
Schmidt, A.C.K., Science, M., Brickley, P., Marine, H., 2011. A feature oriented regional modeling system for the North Brazil current rings migration after retroflection. Offshore Technology Conference.
Schmitz Jr., W.J., McCartney, M.S., 1993. On the North Atlantic Circulation. Rev. Geophys. 31, 29–49.
Schott, F.A., Dengler, M., Brandt, P., Affler, K., Fischer, J., Bourlès, B., Gouriou, Y., Molinari, R.L., Rhein, M., 2003. The zonal currents and transports at 35 W in the tropical Atlantic. Geophys. Res. Lett. 30, 1349.
Servain, J., Busalacchi, A.J., Mcphaden, M.J., Moura, A.D., Reverdin, G., Vianna, M., Zebiak, S.E., 1998. A pilot research moored array in the tropical Atlantic (PIRATA). Bull. Am. Meteorol. Soc. 79, 2019–2031.
Shchepetkin, A.F., McWilliams, J.C., 2005. The regional oceanic modeling system (ROMS): a split-explicit, free-surface, topography-following-coordinates oceanic model. Ocean Model. (Oxf) 9, 347–404.
Silva, A.C., Araujo, M., Medeiros, C., Silva, M., Bourlès, B., 2005. Seasonal changes in the mixed and barrier layers in the western equatorial Atlantic. Braz. J. Oceanogr. 53 (3/4), 83–98.
Silva, M., Araujo, M., Servain, J., Penven, P., Lentini, C.A.D., 2009a. High-resolution regional ocean dynamics simulation in the southwestern tropical Atlantic. Ocean Model. (Oxf) 30, 256–269.
Silva, A.C., Bourlès, B., Araujo, M., 2009b. Circulation of the thermocline salinity maximum waters off the Northern Brazil as inferred from in situ measurements and numerical results. Ann. Geophys. 27, 1861–1873.
Silva, A.C., Araujo, M., Bourlès, B., 2010. Seasonal variability of the Amazon River plume during REVIZEE program. Trop. Oceanogr. 38, 70–81.
Smith, W.H.F., Sandwell, D.T., 1997. Global sea floor topography from satellite altimetry and ship depth soundings. Science 80- (277), 1956–1962.
Song, Y., Haidvogel, D.B., 1994. A semi-implicit ocean circulation model using a generalized topography-following coordinate system. J. Comput. Phys. 115, 228–244. https://doi.org/10.1006/jcph.1994.1189.
Sprintall, J., Tomczak, M., 1992. Evidence of the barrier layer in the surface layer of the tropics. J. Geophys. Res. Oceans 97, 7305–7316.
Stramma, L., Rhein, M., Brandt, P., Dengler, M., Böning, C., Walter, M., 2005. Upper ocean circulation in the western tropical Atlantic in boreal fall 2000. Deep. Sea Res. Part I Oceanogr. Res. Pap. 52, 221–240.
Stukel, M.R., Coles, V.J., Brooks, M.T., Hood, R.R., 2014. Top-down, bottom-up and physical controls on diatom-diazotroph assemblage growth in the Amazon River plume. Biogeosciences 11, 3259–3278.
Tchamabi, C.C., Araujo, M., Silva, M., Bourlès, B., 2017. A study of the Brazilian Fernando de Noronha Island and Rocas Atoll wakes in the tropical Atlantic. Ocean Model. (Oxf). https://doi.org/10.1016/j.ocemod.2016.12.009.
Veleda, D., Araujo, M., Zantopp, R., Montagne, R., 2012. Intraseasonal variability of the North Brazil Undercurrent forced by remote winds. J. Geophys. Res. 117, C11024.
Wang, Y., 2004. Ocean Tide Modeling in the Southern Ocean. Technical Report 471. Department of Civil and Environmental Engineering and Geodetic Science. The Ohio State University, Columbus, Ohio.
Xie, S.P., Carton, J.A., 2004. Tropical Atlantic variability: Patterns, mechanisms, and impacts. Earths Climate: The Ocean–Atmosphere Interaction. Geophys. Monogr 147 (100), 121–142. https://doi.org/10.1029/147GM07. Amer. Geophys. Union.